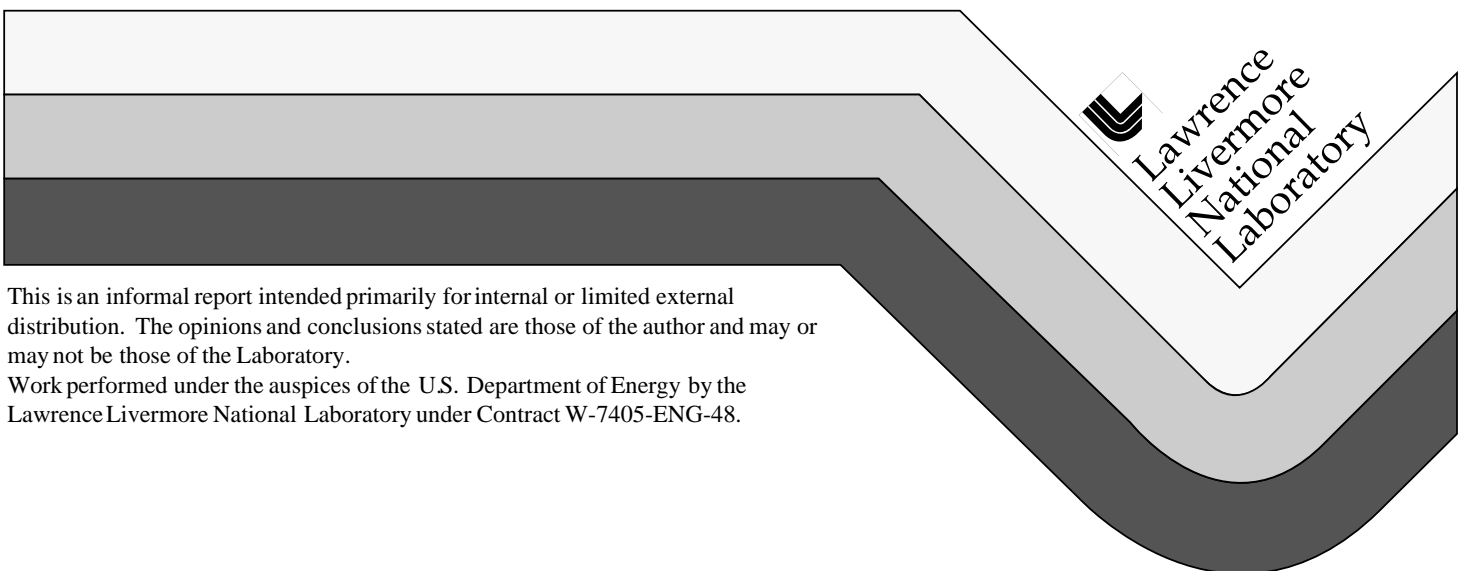


# Description of a Solar Radiative Transfer Model for Use in LLNL Climate and Atmospheric Chemistry Studies

K.E. Grant  
A.S. Grossman

January 7, 1998



This is an informal report intended primarily for internal or limited external distribution. The opinions and conclusions stated are those of the author and may or may not be those of the Laboratory.

Work performed under the auspices of the U.S. Department of Energy by the Lawrence Livermore National Laboratory under Contract W-7405-ENG-48.

#### DISCLAIMER

This document was prepared as an account of work sponsored by an agency of the United States Government. Neither the United States Government nor the University of California nor any of their employees, makes any warranty, express or implied, or assumes any legal liability or responsibility for the accuracy, completeness, or usefulness of any information, apparatus, product, or process disclosed, or represents that its use would not infringe privately owned rights. Reference herein to any specific commercial product, process, or service by trade name, trademark, manufacturer, or otherwise, does not necessarily constitute or imply its endorsement, recommendation, or favoring by the United States Government or the University of California. The views and opinions of authors expressed herein do not necessarily state or reflect those of the United States Government or the University of California, and shall not be used for advertising or product endorsement purposes.

This report has been reproduced  
directly from the best available copy.

Available to DOE and DOE contractors from the  
Office of Scientific and Technical Information  
P.O. Box 62, Oak Ridge, TN 37831  
Prices available from (423) 576-8401

Available to the public from the  
National Technical Information Service  
U.S. Department of Commerce  
5285 Port Royal Rd.,  
Springfield, VA 22161

# **Description of a Solar Radiative Transfer Model for Use in LLNL Climate and Atmospheric Chemistry Studies**

Keith Eric Grant and Allen S. Grossman  
(keg@llnl.gov)

Atmospheric Science Division  
Lawrence Livermore National Laboratory  
Livermore, CA 94551

7 January 1998

## **Abstract**

This report discusses a solar radiation transfer model developed for use in atmospheric climate and chemistry modeling. Major computational concepts used to facilitate the use of the model for multiple projects are presented. Methods and results used for development of band-average absorption and scattering coefficients are presented. Transmissivities calculated using band-average values are compared with those from more detailed calculations. We present the mathematics underlying the two-stream radiative transfer engine. A spherical atmosphere treatment of the direct solar beam is presented. Finally, we compare the model against several benchmark calculations.

## **1. Introduction**

This report discusses the algorithms and implementation of the basic components of a solar radiative transfer model for use in atmospheric climate and chemistry modeling. Vertical profiles of heating rates obtained from such radiative transfer calculations are an essential part of calculating large-scale and convective atmospheric transport processes. The radiative surface fluxes are a major component of the surface energy balance. In atmospheric chemistry models, spectrally detailed calculations are required to calculate spatial distributions of coefficients for photolysis reactions. In addition to ambient calculations, solar radiative transfer calculations are needed in estimating the direct radiative forcing due to anthropogenic increases in trace gases and aerosols and the indirect forcing from corresponding changes in cloud physical and optical properties.

While much of the discussion in this report of techniques for the solution of the radiative transfer is specific to the use of two-stream algorithms, discussions of the radiative transfer model interface and of the parameterization of optical properties is general. One specific change in the physical specification of bulk optical properties for higher order methods would be to replace all mentions below of “asymmetry parameters” with the more general term “scattering phase function coefficients”. The choice of two-stream algorithms has been mandated by the cost of performing radiative transfer calculations within the context of a three-dimensional global climate or chemistry model. The accuracy of such calculations can be estimated by offline calculations using higher order methods. This has been done by King and Harshvardhan (1986), using the general formulation of two-stream methods presented by Meador and Weaver (1980).

## **2. The Interface Between the External and Solar Radiation Transfer Models**

In implementing the solar radiative transfer model (SRTM) described in this report, we have taken a modular approach that allows its use in a number of applications. These applications include stand-alone calculations of trace gas, aerosol, or cloud radiative forcings, operation within the framework of climate and chemistry models to calculate heating rates, and application within a chemistry model to calculate photodissociation

rates. To accomplish our goal of a portable sub-model, we have divided the modular components into interface routines, server routines and a radiative transfer solution engine. An overview of the model organization we use both to communicate and encapsulate data is given in Figure 1.

The radiative transfer interface routines (RTIRs) communicate between the larger (external) model, such as a climate or chemistry model and the solar radiation model. Implicit to this communication is the isolation of information into specific domains where it is needed. It is this encapsulation of knowledge that allows the radiation model to be used in different contexts with only superficial interface changes. Most communication between the external model and the radiation model is top-down through an interface routine.

Server routines provide information needed for the radiative transfer calculations that create unnecessary complexity in the top down interface. They serve to isolate details of data production from the RTIRs. This might include climatological information brought in periodically from a file or parameterizations of cloud or aerosol optical properties. The server paradigm allows the radiative transfer interface to query the server routine which can use files or global variables shared with the external model to fulfill the request.

## 2.1 The Physical Property Interface

The physical property interface accepts trace gas mixing ratios, aerosol amounts, and cloud types and fractions from the external climate or chemistry model or stand-alone driver. It returns the resulting fluxes and heating rates back to the external model.

In external models that communicate via global variables or common blocks, the physical property interface acts to separate information specific to a particular external model from the underlying structure of the SRTM. This interface passes collected information by argument to the optical property driver. This allows the structure of the optical property driver to be general enough to use in multiple external models with only minor modifications. In chemistry models, there will be two sets of interfaces, one for calculating heating rates and one for calculating photolysis rates.

### Physical Property Interface

This is the interface between the solar radiation package and the external atmospheric climate or chemistry model. It communicates with the external model via calling arguments and/or global variable blocks. It passes physical properties via arguments to the optical property driver. The physical property driver has no information regarding optical properties or wavelength information. It receives back radiative fluxes or heating rates from the optical property driver.

### Optical Property Driver

This optical property driver produces optical properties for  $L \times M$  columns of  $N$  vertical layers, based on input physical properties. No wavelength specific information is allowed outside of this driver and its server routines. The driver passes optical properties to the radiation solver engine and passes resulting fluxes and heating rates back to the physical property interface.

### Radiation Solver Engine

The radiation solver engine implements a specific radiation transfer solution scheme (e.g. two-stream, delta-four-stream, ...). It requires layer optical properties as input and returns fluxes at  $N$  model vertical levels for  $L \times M$  horizontal column problems. It has no knowledge of wavelength or physical property information.

**Figure 1: The structure and data encapsulation properties of the solar radiation driver interface design**

## 2.2 The Optical Property Driver

Only the optical property driver (OPD) has access to information both about the horizontal zones of the external model and the wavelength binning structure of the calculation. The OPD takes physical information such as ozone mixing ratio, cloud liquid water path, and cloud fraction at each horizontal zone and vertical layer and generates composite optical properties such as optical depths, single-scattering albedos, and asymmetry factors. The optical properties are composites, in that they include the contributions of all optically active constituents, such as gaseous absorption, molecular scattering, and absorption and scattering by aerosols and clouds. Because the optical properties vary with wavelength as well as with horizontal location and vertical layers, there are  $L \times M$  separate column problems to solve, where  $L$  is the number of wavelength bins and  $M$  is the number of horizontal cells. The optical properties generated by the internal interface are contained in two-dimensional arrays, having the first dimension  $L \times M$  and a second dimension equal to the number of vertical layers,  $N$ .

This data structure eliminates any need for the solution engine to know either about the wavelength structure or the horizontal structure of the problem. All that the solution engine requires is the vertical grid information for  $L \times M$  separate column problems. This allows the same solution engine to be used for both heating rate and photolysis calculations, even though the two calculations have different spectral ranges and resolutions.

## 3. Spectral Resolution

There are currently two spectral variants of the SRTM. The solar heating rate model covers the spectral region from 0.175  $\mu\text{m}$  to 4  $\mu\text{m}$ . It has nine bands covering the UV-visible region from 0.175  $\mu\text{m}$  to 0.700  $\mu\text{m}$  and three bands resolving H<sub>2</sub>O absorption in the near-IR between 0.700 and 4.0  $\mu\text{m}$ . The photodissociation model covers the spectral region from 0.175  $\mu\text{m}$  to 0.725  $\mu\text{m}$  in 126 bands. Because the spectral details of the model are encapsulated within the optical property driver and are implemented entirely as files included by the compiler or preprocessor, the coding of separate interfaces for heating and photolysis that use the same

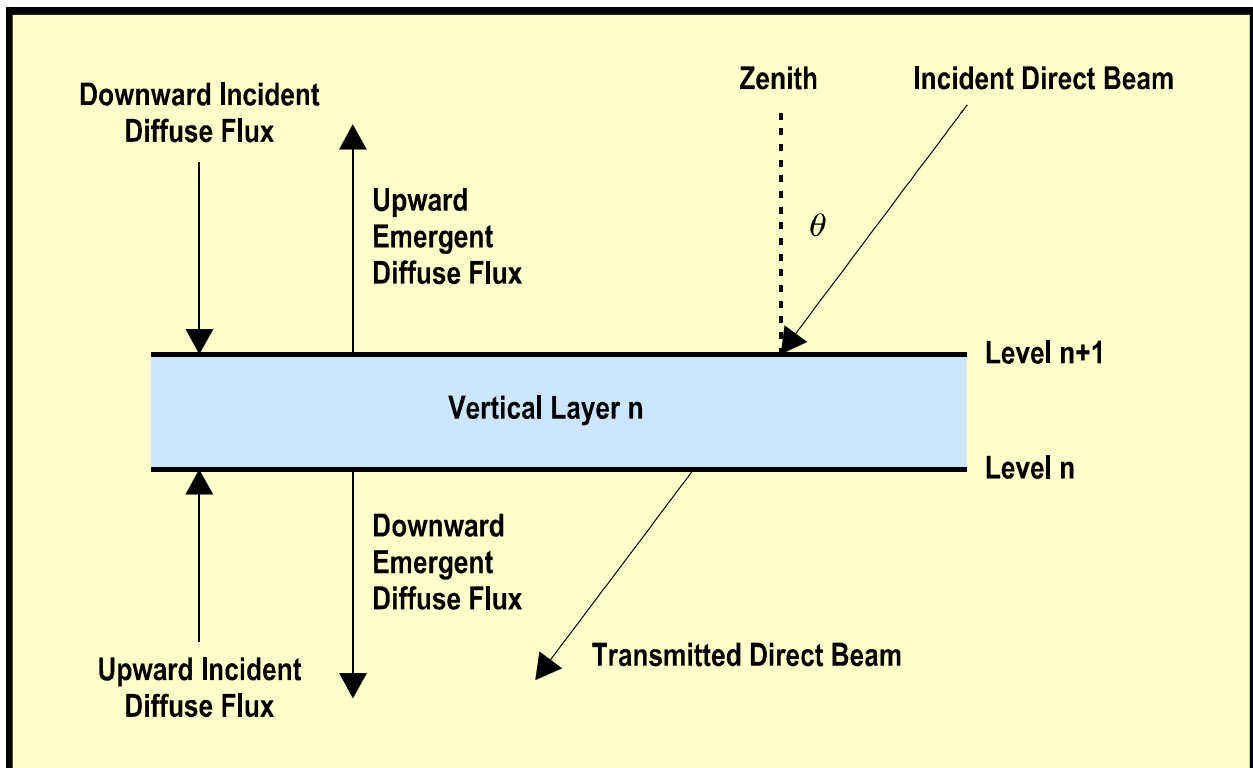


Figure 2: Geometry of the two-stream solar radiative transfer problem for a single atmospheric layer

solution engine is greatly simplified. The use of separate interfaces simply requires having parallel include files with distinct names.

#### 4. UV-Visible Absorption and Rayleigh Scattering

In a manner similar to Chou (1992), coefficients for absorption by ozone and molecular oxygen and for Rayleigh scattering were calculated for each of nine UV-visible bands. Molecular oxygen absorbs only in the first two of these bands and is only important in the upper stratosphere. Because the spectral dependence is much smoother and has much less variance than in the near-IR, only single extinction coefficients are needed for each interaction within a band. For the 126 band photolysis model, simple averages were used for the absorption coefficients. For the nine-band model for UV-visible heating, the best coefficient  $\bar{k}$  for each interaction and band was estimated by a least squares fit over the expected range of absorber path lengths. These average coefficients were determined from

$$e^{-\bar{k}u} = \frac{\int_{\Delta\nu} S_\nu e^{-k_\nu u} d\nu}{\int_{\Delta\nu} S_\nu d\nu}, \quad (1)$$

where  $u$  is the path absorber amount and  $S_\nu$  is the spectral solar flux at the top of the atmosphere. Bands were chosen to facilitate accuracy of overlapping and to keep the range of absorber variation within a band small. The data for the detailed spectral dependence of ozone and molecular oxygen absorption and Rayleigh scattering coefficients was taken from WMO (1985). The spectral dependence of several radiatively important atmospheric constituents is shown in Figure 3. Comparisons of transmissivities computed from the detailed data with those from band averages are shown in Figures 4, 5, and 6, for ozone, Rayleigh scattering, and molecular oxygen. Accuracy is such that the approximate transmissions, in these figures, are barely discernable from the more exact transmissions. The UV-visible band wavelength ranges, top-of-the-atmosphere solar fluxes, and extinction coefficients for ozone and molecular oxygen absorption and for Rayleigh scattering are given in Table 1.

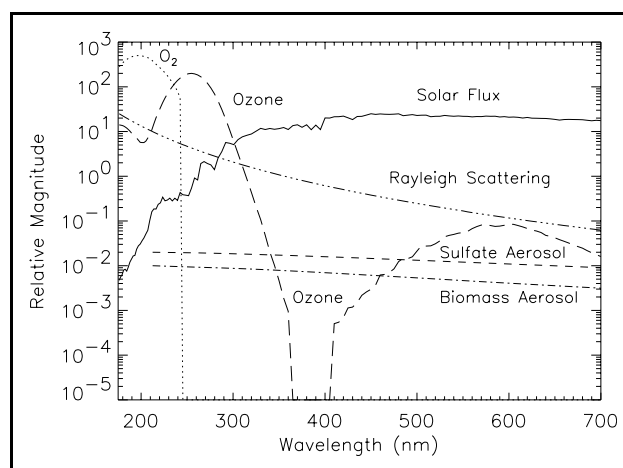


**Figure 3:** Relative spectral variation of UV-visible solar flux and extinction coefficients of various atmospheric constituents. The vertical placement of individual curves is arbitrary.

#### 5. Near-Infrared Water Vapor Absorption

The treatment of the near-IR water vapor absorption is complicated by the wide range of absorption coefficients within each band. The spectral line structure of  $H_2O$  within each band requires a multiple term k-distribution to accurately model the transmission as the path amount of  $H_2O$  increases. This is because line centers saturate as the  $H_2O$  path length increases while line wings are only starting to absorb effectively.

Chou (1986) provided a parameterization for seven flux-weighted k-distribution bands in the near-IR. While providing substantially better spectral resolution than previous one-band near-IR parameterizations, direct use of the seven-band parameterization was undesirable, since it contained 199 separate absorption terms. To reduce the total number of absorption terms, we first combined several of the original bands. Since these bands were all defined in terms of weighted k-distributions, with identical k's in each band, combining bands was accomplished simply by adjusting the weighting factors.

We next used the formalism of the correlated k-distribution method (Grossman and Grant; 1994) to express the weighting of each absorption coefficient in terms of the cumulative probability distribution function. This formalism facilitated using a solar-flux weighted least squares fit to band transmission, as described by Chou (1992) and defined by Eqn. 1, to combine adjacent terms in the probability sum for each band. Such coalescence was terminated when it would have exceeded error criteria for the total band transmission. The final parameterization resulted in three bands containing 15 total terms. Wavelength limits and incident solar fluxes for each near-IR band, as well as k-distribution weights and absorption coefficients, are shown in Table 2. Specifications for a single-band near-IR parameterization are also shown in Table 2.

More specifically, for each band, we transformed from  $dS / d\log(k)$  versus  $\log(k)$  as given by Chou (1986) (where  $S$  is the incident solar flux in the band) to  $k$  versus  $S \Delta G$ , where  $G$  is the cumulative probability distribution. Starting with this initial table of  $k$  versus  $S \Delta G$  for a band, the number of absorption terms was iteratively reduced. For each pair of adjacent  $\Delta G$  intervals, we estimated the flux-weighted transmission error that would be produced by coalescing the two intervals into a single interval with an average absorption coefficient  $\bar{k}$ . The best value for  $\bar{k}$  for each interval pair was estimated by doing a least-squares fit over a range of  $H_2O$  amounts between 0.001 and 10  $g\ cm^{-2}$ . Finally, the interval pair producing the least maximum error was coalesced. This procedure was repeated until further combining of intervals would have exceeded a preset error limit. Transmissions calculated using the full tables of Chou (1986) are compared with those calculated using the economized k-distributions in Figure 7.

## 6. Aerosol Optical Properties

Because the optical depth of aerosols is anticipated to be much less than that for  $O_3$  or  $H_2O$  absorption, simple flux-weighted (Chandrasekhar) means were used to average aerosol properties over each of the 12 spectral bands. Mie calculations producing spectrally detailed specific extinctions, single-scattering albedos, and asymmetry factors were done based on specifications of the aerosol composition and size distribution. The averages of the single-scattering albedos were weighted by both the incident spectral solar flux and the corresponding aerosol specific extinction. The averages of the aerosol asymmetry factors were weighted by the product of the solar flux, the spectral extinction, and the single-scattering albedo. Grant et al. (1996) consider the spectral resolution required to accurately model UV-visible aerosol radiative forcing. This is often a more stringent requirement than that needed for the ambient absorption calculations discussed in Stamnes and Tsay (1990) and Chou (1992). Further discussion of the parameterization of sulfate and carbonaceous aerosol optical properties is pursued in Grant et al. (1997).

## 7. The Two-Stream Solution Method

The solar radiative transfer model uses a two-stream solution algorithm incorporating a layer adding technique to evaluate the fluxes at layer edges. A spherical atmosphere treatment of the path of the direct solar beam (discussed below) is done for large solar zenith angles. The spherical treatment includes effective direct beam extinction by partially cloudy layers. A plane parallel treatment of multiple scattering is used. Sources of diffuse radiation are calculated using the delta-Eddington algorithm described by Joseph and Wiscombe (1976). Error estimates for this algorithm are given by King and Harshvardhan (1986). Reflection and transmission of diffuse radiation are calculated using the algorithm given by Sagan and Pollack (1967).

In calculating the direct-beam radiation multiply scattered by each layer, the optical properties of the different radiatively active components in each atmospheric layer must first be combined into a single set of bulk optical properties. The resulting total optical depth, effective single-scattering albedo, and effective asymmetry factor are defined by the summations

$$\begin{aligned}
\tau &= \sum_i \tau_i \\
\omega_0 \tau &= \sum_i (\omega_0)_i \tau_i \\
g \omega_0 \tau &= \sum_i g_i (\omega_0)_i \tau_i \quad .
\end{aligned} \tag{2}$$

Next, the optical depth  $\tau$ , the albedo for single-scattering  $\omega_0$ , and the asymmetry factor  $g$  are transformed to treat light scattered into the forward diffraction peak as unscattered. This so-called delta-scaling is given by

$$\begin{aligned}
\tau' &= (1 - \omega_0 g^2) \tau \\
\omega_0' &= \frac{(1 - g^2) \omega_0}{1 - \omega_0 g^2} \\
g' &= g / (1 + g) \quad .
\end{aligned} \tag{3}$$

While the delta-scaling reduces the fraction of the light treated as having been scattered from the direct beam, it preserves the amount of light absorbed from the beam. Next, the auxiliary definitions shown in Equations (4) and (5) and are made:

$$\begin{aligned}
\gamma_1 &= (1/4)[7 - \omega_0'(4 + 3g')] \\
\gamma_2 &= -(1/4)[1 - \omega_0'(4 - 3g')] \\
\gamma_3 &= (1/4)(2 - 3g'\mu_0) \\
\gamma_4 &= 1 - \gamma_3
\end{aligned} \tag{4}$$

$$\begin{aligned}
\alpha_1 &= \gamma_1 \gamma_4 + \gamma_2 \gamma_3 \\
\alpha_2 &= \gamma_1 \gamma_3 + \gamma_2 \gamma_4 \\
k &= (\gamma_1^2 - \gamma_2^2)^{\frac{1}{2}}
\end{aligned} \tag{5}$$

Finally the back and forward scattered sources of diffuse radiation (per unit incident direct flux) are given respectively by

$$\begin{aligned}
S_n^b &= \frac{\omega_0'[(1 - k\mu_0)(\alpha_2 + k\gamma_3) - (1 + k\mu_0)(\alpha_2 - k\gamma_3)e^{-2k\tau'} - 2k(\gamma_3 - \alpha_2\mu_0)e^{-\tau'/\mu_0}e^{-k\tau'}]}{(1 - k^2\mu_0^2)[(k + \gamma_1) + (k - \gamma_1)e^{-2k\tau'}]} \\
S_n^f &= \frac{-\omega_0'[(1 + k\mu_0)(\alpha_1 + k\gamma_4)e^{-\tau'/\mu_0} - (1 - k\mu_0)(\alpha_1 - k\gamma_4)e^{-\tau'/\mu_0}e^{-2k\tau'} - 2k(\gamma_4 + \alpha_1\mu_0)e^{-k\tau'}]}{(1 - k^2\mu_0^2)[(k + \gamma_1) + (k - \gamma_1)e^{-2k\tau'}]} \quad .
\end{aligned} \tag{6}$$

The single-layer treatment for incident diffuse irradiance is simpler than that for the direct beam. With the direct beam, it was necessary to account for the dependence on solar zenith angle. With the diffuse irradiance, a constant diffusivity factor can be used. This allows use of the Sagan-Pollack model to calculate layer reflection and transmission factors for diffuse irradiance. Specifically, the reflection and transmission,  $R_n$  and  $T_n$ , of diffuse irradiance by the  $n^{\text{th}}$  layer are given by:

$$\begin{aligned}
u_n &= \sqrt{\frac{1 - \omega_0 g}{1 - \omega_0}}, \\
R_n &= \frac{(u_n^2 - 1) \left( 1 - e^{-2\tau \sqrt{3(1 - \omega_0 g)(1 - \omega_0)}} \right)}{(u_n + 1)^2 - (u_n - 1)^2 e^{-2\tau \sqrt{3(1 - \omega_0 g)(1 - \omega_0)}}}, \\
T_n &= \frac{4u_n e^{-\tau \sqrt{3(1 - \omega_0 g)(1 - \omega_0)}}}{(u_n + 1)^2 - (u_n - 1)^2 e^{-2\tau \sqrt{3(1 - \omega_0 g)(1 - \omega_0)}}}.
\end{aligned} \tag{7}$$

For each layer, reflection and transmission fractions, upwards and downwards source fractions, and the direct beam transmission are calculated both for a cloud-free layer and for a totally cloudy layer.

Cloud optical properties (optical depth, single scattering albedo, and asymmetry factor) are parameterized as functions of model layer and wavelength. Cloud overlap is treated by linearly averaging each reflection, transmission, source, or beam transmission operator proportionally to the fractional cloudiness assigned to the layer. This technique is similar to the method suggested by Morcrette and Fouquart (1986) and Fouquart and Bonnel (1980). It is logically equivalent to the random cloud-overlap assumption, with the advantage of requiring only one column flux calculation.

Using the spherical atmosphere direct beam treatment (after averaging for fractional cloudiness), the direct beam flux transmitted from the top of the atmosphere to the current layer is calculated. Because of the spherical treatment, the direct beam can, depending on solar zenith angle, have both downwards and upwards components. The upwards and downwards fluxes at each level are then calculated from the diffuse reflection, diffuse transmission and source (diffuse radiation scattered from the direct beam) operators using a layer adding algorithm. This algorithm, a simplification for two-stream flux calculations of the more general algorithm of Grant and Hunt (1969), can be described as follows.

First, we make the following definitions:

- $F_n^{\downarrow 0}$  . . . . The direct-beam solar irradiance downward through level n (solar zenith angles  $< 91^\circ$ ).
- $F_n^{\uparrow 0}$  . . . . The direct-beam solar irradiance upward through level n (solar zenith angles  $> 89^\circ$ ).
- $R_n$  . . . . . The reflectivity of layer n to unit diffuse irradiance.  $R_0$  is defined to be the surface albedo for diffuse irradiance.
- $T_n$  . . . . . The transmissivity of layer n to unit diffuse irradiance.  $T_0$  the transmissivity of the surface to diffuse irradiance, is defined to be zero.
- $S_n^b$  . . . . . The backward source of diffuse irradiance from layer n per unit incident direct solar irradiance incident on layer n.  $S_0^b$  is defined to be the surface albedo for direct solar irradiance. All direct irradiance reflected from the surface is assumed to be converted into diffuse irradiance.
- $S_n^f$  . . . . . The forward source of diffuse irradiance from layer n per unit incident direct solar irradiance incident on layer n.  $S_{N+1}^f$ , the source of diffuse downwelling irradiance at the top of the atmosphere, is defined to be zero.

- $cr_n$  . . . . . The composite reflectivity for diffuse upwards irradiance at level n due to all layers above level n (i.e. layers n through N).
- $M_n$  . . . . . The magnification factor for multiple reflections at level n between layer n-1 and all the layers above level n.
- $D_n^\downarrow$  . . . . . The upwards diffuse radiation through level n, from all sources, that has not previously crossed level n+1.
- $D_n^\uparrow$  . . . . . The downwards diffuse radiation through level n, from all sources, that has not previously crossed level n+1.

The boundary conditions at the surface and at the top of the atmosphere on the layer reflectivity, transmissivity, and source fractions are given by:

$$\begin{aligned}
 R_0 &= \alpha , \\
 T_0 &= 0 , \\
 S_0^b &= \alpha + (1 - \alpha) e^{-0.1(90^\circ - \theta_0)} , \\
 S_{N+1}^f &= 0 ,
 \end{aligned} \tag{8}$$

where  $\alpha$  is the surface albedo for diffuse irradiance and  $\theta_0$  is the solar zenith angle. The parameterization for the direct beam albedo as a function of solar zenith angle is taken from Paltridge and Platt (1976). Using these conditions, the composite reflectivities, magnification factors, and intermediate fluxes are computed. First setting the values at the top of the atmosphere,

$$\begin{aligned}
 cr_{N+1} &= 0 , \\
 M_{N+1} &= 1 , \\
 D_{N+1}^\downarrow &= 0 , \\
 D_{N+1}^\uparrow &= S_{N+1}^\uparrow F_{N+1}^0 .
 \end{aligned} \tag{9}$$

and then progressing by recurrence downward through the atmosphere.

$$\begin{aligned}
 cr_n &= R_n + T_n cr_{n+1} M_{n+1} T_n , \\
 M_n &= (1 - cr_n R_{n-1})^{-1} , \\
 D_n^\downarrow &= [D_{n+1}^\downarrow + (S_n^b F_{n+1}^{0\downarrow} + S_n^f F_n^{0\uparrow}) cr_{n+1}] M_{n+1} T_n + S_n^f F_{n+1}^{0\downarrow} + S_n^b F_n^{0\uparrow} , \\
 D_n^\uparrow &= (D_n^\downarrow R_{n-1} + S_{n-1}^b F_n^{0\downarrow} + S_{n-1}^f F_{n-1}^{0\uparrow}) M_n .
 \end{aligned} \tag{10}$$

On reaching the surface, the upward and downward fluxes are given by:

$$\begin{aligned}
 F_1^\downarrow &= D_1^\downarrow , \\
 F_1^\uparrow &= D_1^\uparrow + F_1^\downarrow cr_1 + F_1^{0\uparrow} .
 \end{aligned} \tag{11}$$

Finally, the complete fluxes at the remaining atmospheric levels are computed, moving upwards through the atmosphere, using the recurrence relations:

$$\begin{aligned}
F_n^\uparrow &= D_n^\uparrow + F_{n-1}^\uparrow T_{n-1} M_n + F_n^{0\uparrow}, \\
F_n^\downarrow &= D_n^\downarrow + (F_n^\uparrow - F_n^{0\uparrow}) cr_n + F_n^{0\downarrow}.
\end{aligned}
\tag{12}$$

The formulation presented above can provide the fluxes at atmospheric levels for a single set of bulk optical properties per layer. This corresponds to a single wavelength bin or a single term in a "k-distribution" expansion. To obtain total fluxes for heating rate calculations, a sum is done overall all such terms. To obtain photodissociation rate coefficients, wavelength dependent actinic fluxes are calculated from the vertical fluxes. Madronich (1987) discusses the subtleties of converting from vertical fluxes to the actinic fluxes required to calculate photodissociation rate. These are then convolved with quantum yields and absorption coefficients for specific reactions.

## 8. Spherical Atmosphere Treatment of the Direct Solar Beam

### 8.1 Direct Beam Path and Extinction

For solar zenith angles approaching or greater than  $90^\circ$ , a purely plane-parallel treatment of the atmospheric radiative transfer problem breaks down. Despite this, the diffuse (i.e. already scattered) radiation can still be treated in a plane parallel approximation to reasonable accuracy.

Whether the solar beam is incident at a zenith angle less than  $90^\circ$ , equal to  $90^\circ$ , or greater than  $90^\circ$ , it will have a point of tangency at which it is parallel to the Earth's surface. The altitude  $Z_{tan}$  of tangency will depend both on the solar zenith angle  $\theta$  and on the point of observation at an altitude  $Z_{obs}$ . Given the radius of the Earth,  $R$ , via use of the law of sines and, for  $\theta > 90^\circ$  the equivalence of  $\sin(\theta)$  and  $\sin(180^\circ - \theta)$ , we can write that

$$Z_{tan} = R \left[ \left( 1 + \frac{Z_{obs}}{R} \right) \sin(\theta) - 1 \right]
\tag{13}$$

For horizontally incident radiation ( $\theta = 90^\circ$ ), we note that Eqn. 13 correctly reduces to  $Z_{tan} = Z_{obs}$ . The distance from the point of tangency at  $Z_{tan}$ , to a point at any higher altitude,  $Z$ , forms a right triangle. Using this, we can write

$$D^2 = (Z + R)^2 - (Z_{tan} + R)^2
\tag{14}$$

The use of Equations 13 and 14 allows us to calculate the distance the solar beam travels as it crosses a concentric shell (layer) of atmosphere between altitudes  $Z$  and  $Z+\Delta Z$ . Having first delta-scaled the optical properties of the layer, we can then calculate the extinction of the solar beam in crossing through the layer.

Another consideration comes in estimating the absorption of the direct solar beam at altitudes above the explicitly modeled atmosphere. Under the assumption of an effectively isothermal atmosphere with constant mixing ratios of absorbing gases above the top of the model atmosphere, we can use the Chapman function (Wilkes, 1954; Green and Martin, 1966) to estimate the path length magnification. Taking the essential part of an expansion given by Green and Martin (1996), we can write

$$M(\theta) = \alpha [(\alpha^2 - 1) \cos^2 \theta + 1]^{-1/2}
\tag{15}$$

for the path magnification factor. Fitting Eqn. 15 to Wilkes (1954) tables for  $R + Z_{\text{TOA}} = 900 H$ , where  $R$  is the Earth's radius,  $Z_{\text{TOA}}$  is the altitude of the top of the modeled atmosphere, and  $H$  is the atmospheric scale height (about 7 km), yields values for  $\alpha$  between 31 to 35, depending on the exact weighting used. Note that Eqn. 15 is still correct for  $\theta > 90^\circ$ , since the angle of incidence of the radiation at the top of the atmosphere is then  $180^\circ - \theta$ .

## 8.2 The Diffuse Radiation Source

We use the plane-parallel delta-Eddington approximation for each layer to calculate the fractional sources of forward and backwards diffuse radiation scattered from the incident solar beam. This approximation cannot handle horizontally incident radiation. Therefore, when the solar zenith angle is between  $89^\circ$  and  $91^\circ$ , we treat the incident radiation as if it were incident at both of these angles. The relative weight given each angle is interpolated based on the cosine of the solar zenith angle.

## 8.3 Calculation of Heating Rates

Generally, in the plane-parallel treatment of atmospheric radiation, heating rates are calculated from the divergence of the net radiative flux between two vertical levels. Implicit in this treatment is the assumption that the difference in flux between the levels is due solely to passage of radiation through the intervening layer. This is true only for a downward incident direct solar beam.

For an upward incident beam, the radiation incident at the bottom of a layer will have penetrated more deeply into the atmosphere (i.e. it will have a lower tangent altitude) than the radiation incident at the top of the layer. Thus the divergence of direct beam flux between the two levels will not correctly account for absorption within the layer. Instead we account for the absorptivity of each layer when using the delta-Eddington approximation to calculate the forward and backward sources of diffuse radiation from the incident solar beam.

## 9. Comparisons with Benchmark Radiative Flux Calculations

In table 3, we compare of results from the current model with those for clear-sky, mid-latitude summer cases from the shortwave ICRCCM (Intercomparison of Radiation Codes for Climate Models) study (Fouquart et al., 1991). In all cases, the errors in the surface downward fluxes and total atmospheric absorption are well within the five to ten percent accuracy expected of a two-stream model (King and Harshvardhan, 1986). The largest errors are seen in the absorption by  $\text{H}_2\text{O}$  for a  $75^\circ$  solar zenith angle. These errors, largely a result of limiting the number of terms used for the near-IR parameterization, are also evident in the transmission error plots in Figure 7 at large absorber path lengths.

## 10. Acknowledgements

Work performed under the auspices of the U.S. Dept. of Energy by the Lawrence Livermore National Laboratory under contract No. W-7405-Eng-48.

## References

Chou, Ming-Dah, 1986: Atmospheric solar heating rates in the water vapor bands, *J. Clim. and Appl. Met.*, **25**, 1532-1542.

- Chou, Ming-Dah, 1992: A solar radiation model for use in climate studies, *J. Atmos. Sci.*, **49**, 762-772.
- Fouquart, Y., and B. Bonnel, 1980: Computation of solar heating of the Earth's atmosphere: a new parameterization, *Contribution to Atmos. Phys.*, **53** (1), 35-62.
- Fouquart, Y., B. Bonnell, and V. Ramaswamy, 1991: Intercomparing Shortwave Radiation Codes for Climate Studies, *J. Geophys. Res.*, **96** (D5), 8955-8968.
- Grant, I.P., and G.E. Hunt, 1969: Discrete space theory of radiative transfer — I. Fundamentals, *Proc. Roy. Soc. Lond. A*, **313**, 183-197.
- Grant, Keith E., Allen S. Grossman, Cathy C. Chuang, and Joyce E. Penner, 1996: Sensitivity of Aerosol Radiative Forcing Calculations to Spectral Resolution, *IRS '96: Current Problems in Atmospheric Radiation — Proceedings of the International Radiation Symposium 1996, 19-24 August 1996, Fairbanks Alaska*, W.L. Smith and K. Stamnes ed., A. Deepak Publishing, Hampton Virginia, 275-278.
- Grant, Keith E., Cathy C. Chuang, Allen S. Grossman, and Joyce E. Penner, 1997: Modeling the Spectral Optical Properties of Ammonium Sulfate and Biomass Burning Aerosols, submitted to *Atmospheric Environment* for the special section on papers from the 6<sup>th</sup> International Conference on Carbonaceous Aerosols, Vienna, Austria.
- Green, A.E.S., and J.D. Martin, 1966: Chapter 7 — A generalized Chapman Function, in *The Middle Ultraviolet: Its Science and Technology*, A.E.S. Green, Editor, John Wiley & Sons, Inc., New York.
- Grossman, A.S., and K.E. Grant, 1994: A correlated k-distribution model of the heating rates for atmospheric mixtures of H<sub>2</sub>O, CO<sub>2</sub>, O<sub>3</sub>, CH<sub>4</sub> and N<sub>2</sub>O in the 0 - 2500 cm<sup>-1</sup> wave number region at altitudes between 0 and 60 km. Proceedings of The 8th Conference on Atmospheric Radiation, American Meteorological Society, Nashville, Tenn., Jan. 23 - 28, 97-99.
- Harshvardhan, Roger Davies, David A. Randall, and Thomas G. Corsetti, 1987: A fast radiation parameterization for atmospheric circulation models, *J. Geophys. Res.*, **92** (D1), 1009-1016.
- Joseph, J.H., and W.J. Wiscombe, 1976: The Delta-Eddington Approximation for Radiative Flux-Transfer, *J. Atmos. Sci.*, **33**, 2452-2459.
- King, Michael D. and Harshvardhan, 1986: Comparative Accuracy of selected multiple scattering approximations, *J. of the Atmos. Sci.*, **43**, 784-801.
- Madronich, Sasha, 1987: Photodissociation in the atmosphere — I. Actinic flux and the effects of ground reflections and clouds, *J. Geophys. Res.*, **92** (D8), 9740-9752.
- Meador, W.E., and W. R. Weaver, 1980: Two-stream approximations to radiative transfer in planetary atmospheres: a unified description of existing methods and a new improvement, *J. of the Atmos. Sci.*, **37**, 630-643.
- Morcrette, Jean-Jacque, and Yves Fouquart, 1986: The overlapping of cloud layers in shortwave radiation parameterizations, *J. of the Atmos. Sci.* **43**, 321-328.
- Paltridge, G.W., and C.M.R. Platt, 1976: *Radiative Processes in Meteorology and Climatology*, Elsevier Scientific Publishing Company, New York.
- Sagan, C., and J.B. Pollack, 1967: Anisotropic nonconservative scattering and the clouds of Venus, *J. Geophys. Res.*, **72**, 469-477.
- Stamnes, K., and S-C. Tsay, 1990: Optimal Spectral Resolution for Computing Atmospheric Heating and Photodissociation Rates, *Planet. Space Sci.*, **38** (6), 807-820.
- Wilkes, M.V., 1954: A table of Chapman's grazing incidence integral  $Ch(x,\gamma)$ , *Proc. Phys. Soc. London*, **V67B**, 304-308.
- WMO, 1985: Reference Solar Irradiance, Rayleigh Scattering, O<sub>2</sub>, and O<sub>3</sub> Cross Sections, *Atmospheric Ozone 1985*, WMO Global Ozone Research and Monitoring Project — Report No. 16, Vol. I., pp. 355-362.

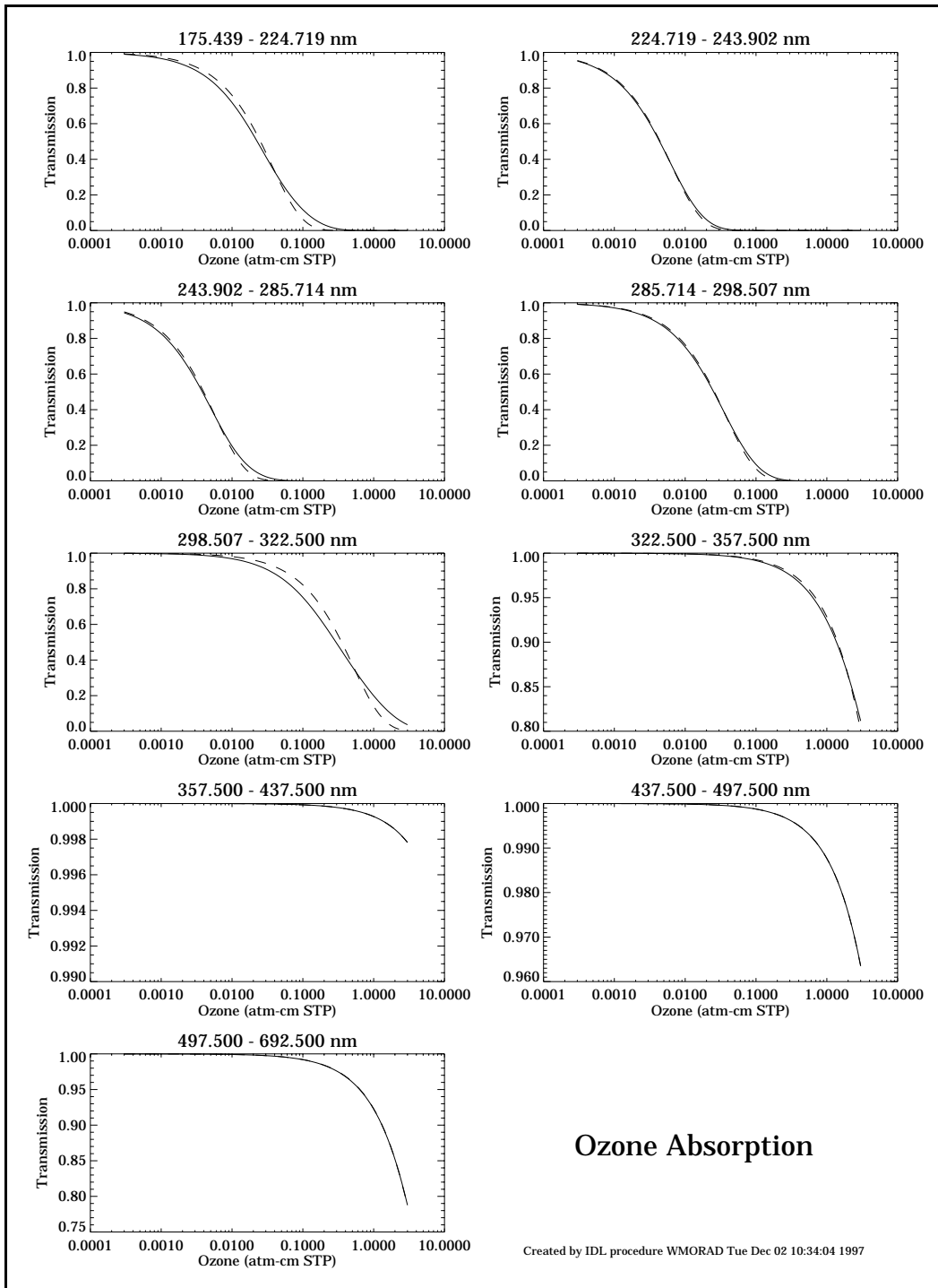


**Figure 4:** Comparison of ozone band transmissions calculated via integrating detailed spectral data (solid lines) with those calculated using single, band-average, absorption coefficients (dashed lines).

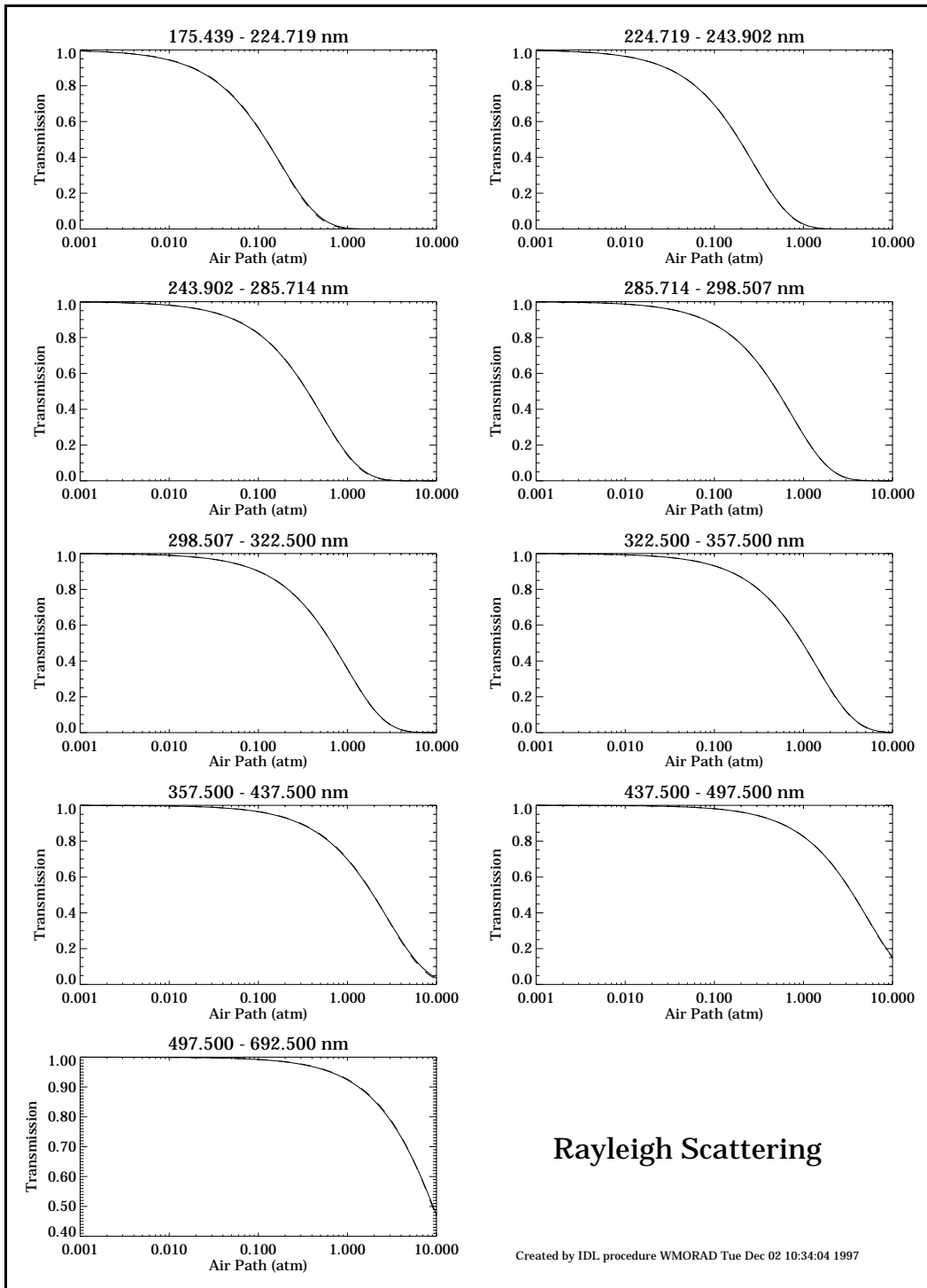


**Figure 5:** Comparison of Rayleigh scattering band transmissions calculated via integrating detailed spectral data (solid lines) with those calculated using single, band-average, scattering coefficients (dashed lines).

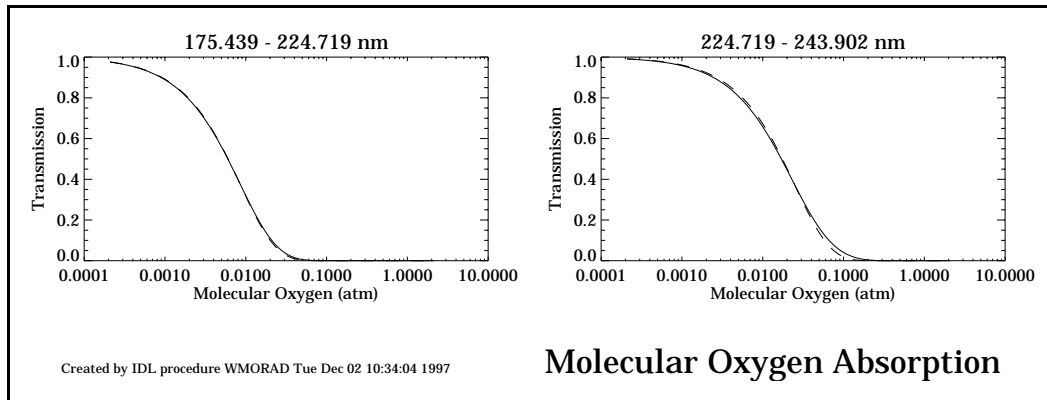


**Figure 6:** Comparison of molecular oxygen band transmissions calculated via integrating detailed spectral data (solid lines) with those calculated using single, band-average, absorption coefficients (dashed lines).

Table 1: Wavelength limits, top-of-the-atmosphere solar fluxes, and extinction coefficients for each UV-visible band and for each absorbing and scattering species.

Band	Wavelength Range (nm)	Flux ( $\text{W m}^{-2}$ )	$k\text{-O}_2$ ( $\text{mb-air}^{-1}$ )	$k\text{-O}_3$ ( $\text{cm}^2 \text{atm-cm}^{-1}$ )	$k\text{-Rayleigh}$ ( $\text{mb-air}^{-1}$ )
1	175.439 – 224.719	7.7030e-01	2.3680e-02	2.7513e+01	5.6179e-03
2	224.719 – 243.902	9.2719e-01	8.1730e-03	1.5643e+02	3.6097e-03
3	243.902 – 285.714	6.3155e+00	0.0000e+00	1.7460e+02	1.9166e-03
4	285.714 – 298.507	6.1310e+00	0.0000e+00	2.6844e+01	1.3378e-03
5	298.507 – 322.500	1.5161e+01	0.0000e+00	1.9620e+00	1.0213e-03
6	322.500 – 357.500	3.3323e+01	0.0000e+00	7.4017e-02	6.9941e-04
7	357.500 – 437.500	1.1133e+02	0.0000e+00	7.2952e-04	3.4971e-04
8	437.500 – 497.500	1.1960e+02	0.0000e+00	1.2394e-02	1.8785e-04
9	497.500 – 692.500	3.3668e+02	0.0000e+00	8.0111e-02	7.6074e-05

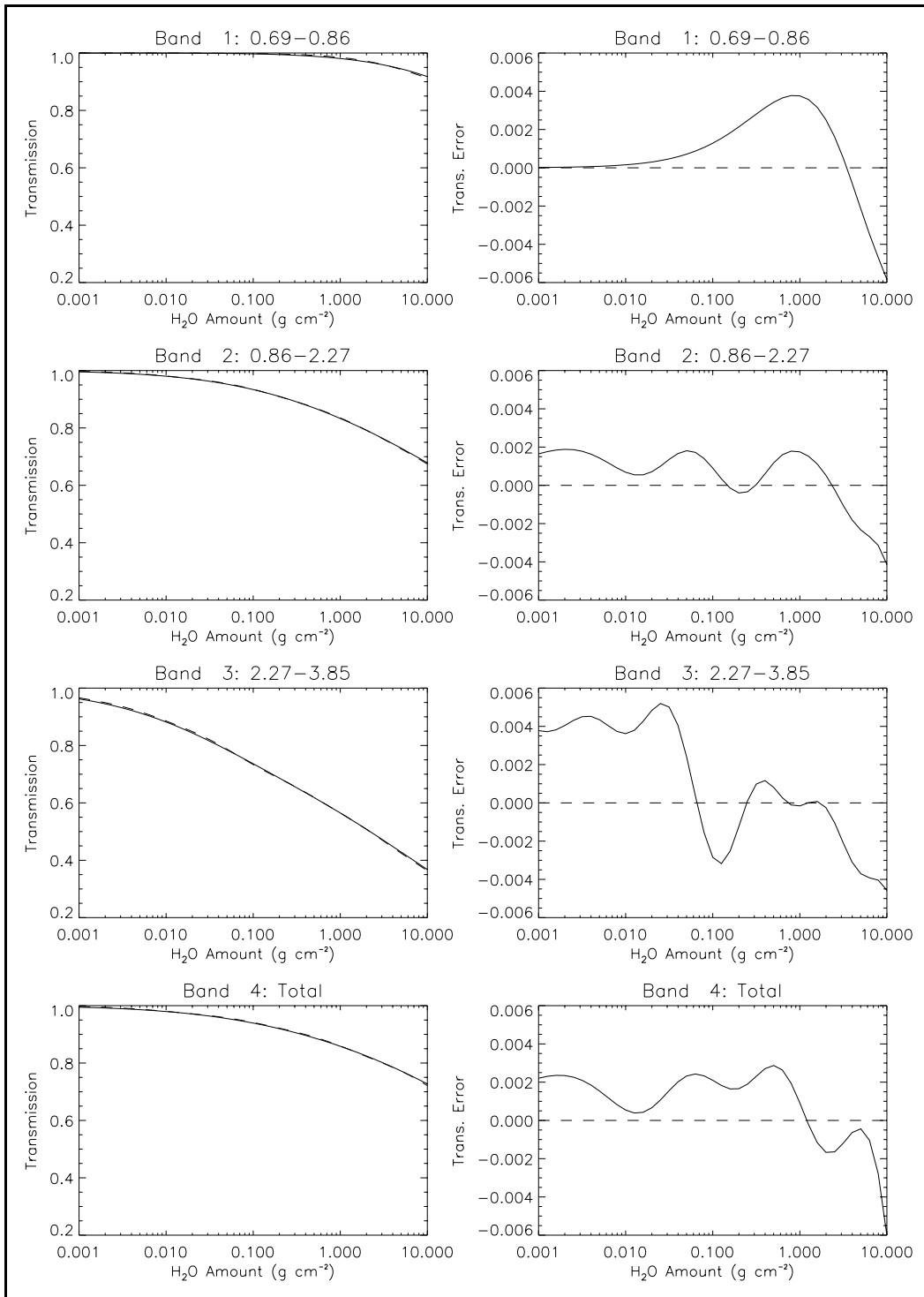


**Figure 7:** Comparison of H<sub>2</sub>O near-IR band transmission calculated using the full k-distribution sets (solid lines) from Chou (1986) with those calculated using the economized k-distribution sets.

Table 2: Near-infrared band wavelength ranges, top-of-the-atmosphere solar fluxes, and individual band k-distribution cumulative probability increments and absorption coefficients are given. Data for the three-band model discussed in the body of the report plus a those single-band combined model are shown. All absorption coefficients are for 240 K and 300 hPa. Chou (1986) provides a scaling to other temperatures and pressures.

Band	1	2	3	Combined Band
Wavelength Range ( $\mu\text{m}$ )	0.69 – 0.86	0.86 – 2.27	2.27 – 3.85	0.69 – 3.85
Solar Flux in Band ( $\text{W m}^{-2}$ )	209.770	472.710	46.788	729.270
$\Delta G_1$	0.948551	0.703232	0.389153	0.790585
$k_1$ ( $\text{cm}^2 \text{g}^{-1}$ )	4.3980e-03	7.6655e-03	1.4989e-02	1.0022e-02
$\Delta G_2$	0.051449	0.085079	0.106278	0.063063
$k_2$ ( $\text{cm}^2 \text{g}^{-1}$ )	2.4676e-01	1.3370e-01	1.3525e-01	2.3374e-01
$\Delta G_3$	—	0.098956	0.142613	0.085075
$k_3$ ( $\text{cm}^2 \text{g}^{-1}$ )	—	5.3350e-01	5.3707e-01	1.1571e+00
$\Delta G_4$	—	0.046725	0.118942	0.042457
$k_4$ ( $\text{cm}^2 \text{g}^{-1}$ )	—	2.3126e+00	3.1426e+00	1.0938e+01
$\Delta G_5$	—	0.049153	0.151376	0.018820
$k_5$ ( $\text{cm}^2 \text{g}^{-1}$ )	—	1.0536e+01	2.1238e+01	1.4219e+02
$\Delta G_6$	—	0.016855	0.068448	—
$k_6$ ( $\text{cm}^2 \text{g}^{-1}$ )	—	1.3122e+02	1.8492e+02	—
$\Delta G_7$	—	—	0.023190	—
$k_7$ ( $\text{cm}^2 \text{g}^{-1}$ )	—	—	1.6292e+03	—

Table 3: Comparison of the solar model for six clear-sky, mid-latitude summer cases from the shortwave Intercomparison of Radiation Codes for Climate Models (ICRCCM). ICRCCM median results (blue) for the downward flux at the surface and total atmospheric absorption are given, along with the corresponding RMS percentage errors. Results from the current solar model (red) are shown along with their percent deviation from the ICRCCM medians. Cases 1 and 2 include H<sub>2</sub>O absorption only. Cases 31 through include Rayleigh scattering and absorption by O<sub>3</sub> O<sub>2</sub>(UV) and H<sub>2</sub>O.

ICRCCM Solar Case	Solar Zenith Angle (deg)	Surface Albedo	Number of Models Compared	Downward flux at the Surface (W m <sup>-2</sup> )	RMS Error in Flux (%)	Atmospheric Absorption (W m <sup>-2</sup> )	RMS Error in Absorption (%)
1	30	0.0	24	1019.0 1012.0	4 -0.69	167.0 165.4	5% -0.96
2	75	0.0	24	289.0 282.4	6 -2.3	64.2 69.5	7 8.2
31	30	0.2	21	943.7 945.7	2 0.21	206.2 208.6	6 1.2
32	30	0.8	21	985.0 988.6	2 0.37	245.3 246.6	5 0.53
33	75	0.2	21	235.8 235.7	2 -0.04	83.8 87.4	5 4.3
34	75	0.8	21	246.2 245.3	4 -0.37	89.2 95.1	7 6.6